



Thermal Analysis of the Gelation Process of Li-ion Battery Polymer Electrolyte by Electron Irradiation Using Multi-physics Simulation

Woojien Lee¹ · Jaehyeon Kim² · Taeshik Earmme² · Kunok Chang¹

Received: 8 June 2024 / Revised: 2 August 2024 / Accepted: 24 August 2024

© The Author(s), under exclusive licence to Korean Institute of Chemical Engineers, Seoul, Korea 2024

Abstract

Rechargeable lithium-based batteries play a crucial role in the shift towards renewable energy, providing eco-friendly alternatives to fossil fuels and improving sustainability. However, their liquid electrolytes present significant safety risks, especially in electric vehicles. To address this, the process of gelation through cross-linking has emerged as a promising solution, effectively reducing the risk of combustion. Traditional gelation methods are time-consuming and costly, often taking up to an hour. In contrast, electron beam irradiation provides a highly efficient alternative, reducing the process to just seconds. This lowers production costs and meets the demands of high-volume manufacturing. In this study, the multiphysical phenomena in the coin cell were simulated using, which combines radiation transport modeling, phase change simulation of the gelation process, and thermal analysis. Through this, the peak temperature of the electrolyte in the coin cell was predicted and the time required for the temperature of the electrolyte to return to the ambient temperature was predicted.

Keywords Electron beam · Rechargeable battery · Polymer electrolyte · Gelation · Phase-field modeling · Multi-physics simulation

Introduction

The advancement of rechargeable lithium-ion batteries (LIBs) is crucial for the shift toward renewable energy [1]. Transformational advancements in battery technologies are essential to facilitate the efficient utilization of renewable energy sources, such as, solar, wind, and hydrogen enabling the proliferation of hybrid electric vehicles (HEVs) into plug-in HEVs and fully electric vehicles [2]. The widespread adoption of LIBs, driven by their convenience and high efficiency, has concurrently raised concerns regarding their safety [3]. The safety of lithium-ion batteries is believed to be closely linked to the internal components, including the electrolyte, cathode material, anode material, separator, and other electronic devices [4]. Among the components of lithium-ion batteries, the electrolyte is considered

to be the most flammable. Consequently, it is closely related to the battery's safety [5].

Research aimed at enhancing the safety of liquid electrolytes has been carried out in various methodologies [6–8]. Among these, the transformation of the liquid electrolyte into gel polymer electrolyte (GPEs) is recognized as an effective way to reduce risks of explosion or fire during accidents, while preserving battery efficiency [9–11]. GPEs can be synthesized using methods such as ultraviolet (UV)-curing [12], solvent-casting [13], thermal processing [14] and electrospinning [15]. Compared to the traditional techniques, the electron irradiation process is proving to be a faster, cleaner, and more effective method as it can be performed without any initiator [16, 17]. Therefore, electron beam synthesis of GPE is suitable for large-scale room-temperature production [18, 19].

The gelation process of liquid electrolytes using electron irradiation still needs to be further characterized, and robust processes must be designed before full-scale commercialization is possible. To date, there has been no comprehensive thermal analysis that includes both electron transport modeling and phase change processes such as gelation induced by electron irradiation. We believe that the multi-physics thermal analysis framework for electrolytes that encompasses

✉ Kunok Chang
kunok.chang@khu.ac.kr

¹ Department of Nuclear Engineering, Kyung Hee University, Yong-in City, Republic of Korea

² Department of Chemical Engineering, Hongik University, Seoul, Republic of Korea

the gelation process and electron irradiation will be important for the analysis of electron-irradiated polymer electrolyte gelation processes in LIBs with different form factors and electrochemical properties. Since it is very difficult to observe the inside of the cell when the electrolyte gelation process using electron beams is taking place [20, 21], it is essential to develop advanced simulation methods.

It is evident that temperature represents a critical factor significantly impacting the performance of LIBs. Moreover, the effects of temperature on these batteries are not uniform; they vary depending on specific conditions and locations. Therefore, it is of the utmost importance to accurately measure the internal temperature of LIBs during the manufacturing process and to gain an understanding of the temperature-related effects to ensure optimal process [22]. In this study, we present a multi-physics simulation framework linking electron transport - gelation process - thermal analysis to analyze the polymer electrolyte gelation process of coin-cell LIBs.

For electron transport modeling, the GEANT4 package [23] is used to evaluate the deposited energy by location in LIBs based on absorbed dose from electron radiation. The phase-field methodology [24] is applied to simulate the gelation process utilizing COMSOL based on energy deposited by location from electron transport modeling, and thermal analysis is performed along with it.

Multiphysics simulations that combine electron transport modeling, phase transformation of polymers at the mesoscale with macroscopic thermal analysis have not been attempted before, and this study is significant because it quantitatively assesses the phase transformation of materials due to radiation and how it affects thermal analysis, which is important for process design.

Background for Structure of the Lithium Ion Battery and Manufacture Process

This section includes the basic structure of the LIB and a brief description of the LIB manufacturing process.

Coin-Cell Battery

For the lab-scale experiments, we select coin-cell batteries due to their convenient manufacturing process. These batteries consist of various components such as cathodes, anodes, separators, electrolytes, springs, and gaskets. The dimensions are a diameter of 20 mm and a height of 3.229 mm. The specific sizes and materials of the internal components are detailed in Table 1. The schematic of the coin-cell battery fabricated and used in the experiments is shown in Fig. 1.

Table 1 Coin-cell battery component specifications

Component	Thickness	Outer diameter	Inner diameter	Material
Cap (1)	0.250 mm	18.5 mm	17.2 mm	SUS 316 L
Cap (2)	0.250 mm	16.5 mm	15.8 mm	SUS 316 L
Spring	0.722 mm	14.5 mm	10.5 mm	SUS 316 L
Spacer	1.0 mm	16.0 mm	–	SUS 316 L
Anode	1.0 mm	16.0 mm	–	Lithium metal
Gasket	2.4 mm	19.0 mm	17.0 mm	Poly(propylene)
Separator	15 μ m	18.0 mm	–	Poly(propylene)
Cathode	50 μ m	14.0 mm	–	NCM811, CB, PVDF, Al foil
Case	0.250 mm	20.0 mm	19.5 mm	SUS 316 L

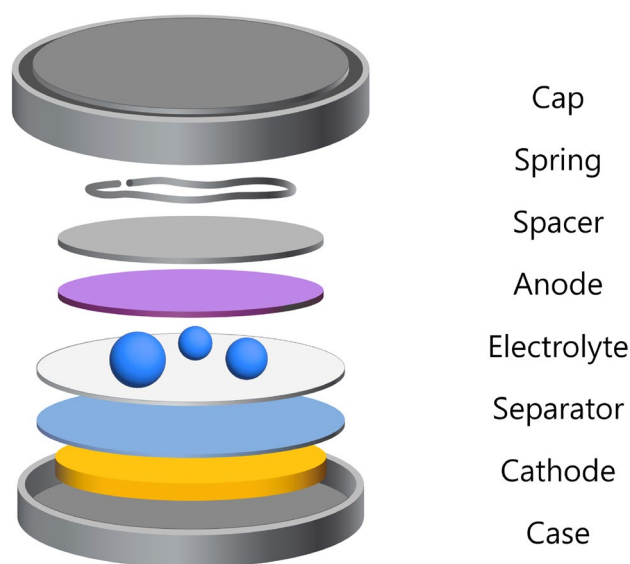


Fig. 1 Schematics of coin-cell battery

The internal components in the coin cell need to be arranged in the correct order as shown in Fig. 1, which is then filled with liquid electrolyte. The liquid electrolyte is exposed to electron beams to solidify, causing the height of the electrolyte region to increase from 3.229 mm to 3.352 mm.

Electrolyte

The electrolyte is a critical component in determining the performance of LIBs, and the choice and combination of materials used are of utmost importance. In this study, a substance convertible to GPEs through radiation exposure is utilized. The electrolyte used in the experiment consists of 1 M lithium bis(trifluoromethanesulfonyl)imide (LiTFSI) in 85%

ethylene carbonate/ethyl methyl carbonate (EC/EMC) and 15% ethoxylated trimethylolpropane triacrylate (ETPTA).

Furthermore, as this substance is a newly developed material, its thermal and material properties required for subsequent simulations are experimentally determined. The measured values are presented in Table 2. The thermal conductivity ($k(T)$) of the LE is calculated using the Eq. 1, wherein the specific heat ($C_p(T)$) and thermal diffusivity ($\alpha(T)$ [m²/sec]) of the sample are determined using a Laser Flash Apparatus (LFA 457, NETZSCH). Similarly, the thermal conductivity of the GPE is calculated using the aforementioned equation (Eq. 1). The specific heat of the GPE is determined via the 3-Run Method using a Differential Scanning Calorimeter (DSC 25, TA Instruments), and the thermal diffusivity is measured using a Laser Flash Apparatus (LFA 457, NETZSCH). For both measurements, the laser voltage of the LFA is set to 230 V, and the pulse width is 0.30 ms. It is observed that as the liquid transforms into a gel state, there is a slight increase in density and a minor enhancement in thermal conductivity.

$$k(T) = \alpha(T) \cdot C_p(T) \cdot \rho(T) \tag{1}$$

Cathode

The cathode material used consists of LiNi_{0.8}Co_{0.1}Mn_{0.1}O₂ (NCM811), carbon black, and polyvinylidene fluoride (PVDF) in a mass ratio of 8:1:1. The current collector is an aluminum foil with a thickness of 15 μm, and the active material loading is 2 mg/cm². The total thickness of the cathode is 50 μm, of which 35 μm comprised the NCM811, carbon black, and PVDF mixture. As the mixture is not free-standing, the material properties are measured in conjunction with the aluminum foil. The specifics regarding the cathode are illustrated in Fig. 2. The material properties of the cathode used for the subsequent simulations are as follows: a density of 1848 kg/m³, a heat capacity of 768 J/kg·K, and a thermal conductivity of 83.7 W/m·K.

Experimental Environment

The experimental setup for electron beam irradiation is described as follows: an electron beam with an energy of 2.5 MeV is used to irradiate the system. The coin-cell battery is

Table 2 Thermal properties of electrolyte

Thermal property	Liquid polymer electrolyte (LE)	Gel polymer electrolyte (GPE)
Density [kg/m ³]	$\rho_{liq} = 1211$	$\rho_{gel} = 1407$
Heat capacity [J/(kg·K)]	$C_{p,liq} = 1552$	$C_{p,gel} = 1520$
Thermal conductivity [W/(m·K)]	$k_{liq} = 0.145$	$k_{gel} = 0.17$

positioned on a rotating rail, which operates at a velocity of 0.283m/s. The dwell time of the coin cell on the rail for the liquid electrolyte gelation process by electron irradiation is about 3 min and 50 s. The electron beam is directed from a height of 35 cm above the rail, and the irradiation zone measures 7.5 cm in width and 150 cm in length. Based on these dimensions, the time that the coin cell is irradiated with electron beams calculates to be 5.3 sec. The experimental facility is designed so that the absorbed dose is 10 kGy when the coin-cell is irradiated once via rail. However, since it is not possible to link electron transport and thermal analysis in real time, this study calculates the energy deposited by electron transport according to the location, and based on this, only thermal analysis is performed for 5.3 sec to release the deposited energy, and after 5.3 sec, thermal analysis and gelation process are simulated simultaneously.

Multiphysics Simulation Strategy

This multiphysics simulation consists of four main simulations. First the electron transport modeling (referred to as ET in Table 3) is performed to obtain the energy deposited in the electrolyte in the coin cell at various locations over 5.3 sec of electron irradiation. These simulations are performed utilizing a package called GEANT4, the details of which are described in sect. 3.1 below.



Fig. 2 Illustration of cathode

Table 3 The multiphysics simulation strategy adopted in the study, $E(\vec{r})$ is the deposited energy within LIB, $E^d(\vec{r})$ is the deposited energy at position \vec{r} during the electron irradiation and $\eta(\vec{r}, t)$ is the degree of gelation, $\eta(\vec{r}, t) = 0$ means liquid electrolyte and $\eta(\vec{r}, t) = 1$ means the gel electrolyte and a value between 0 and 1 indicates the interface between the liquid and gel electrolytes. $T(\vec{r}, t)$ is the temperature of electrolyte function of position and time

Abbr	Name	Software	Input	Output
ET	Electron transport	GEANT4	Number of electrons, Initial kinetic energy	$E(\vec{r})$
TA-1	Thermal analysis	COMSOL	$E^d(\vec{r})$	$T(\vec{r}, t)$
PF	Phase-field modeling of gelation Process	COMSOL	$\lambda(\vec{r})$	$\eta(\vec{r}, t)$
TA-2	Thermal analysis	COMSOL	$\eta(\vec{r}, t)$	$T(\vec{r}, t)$

By electron transport (ET) modeling in Table 3, we evaluate deposited energy $E^d(\vec{r})$ by

$$E^d(\vec{r}) = \int_0^t E(\vec{r}_i, t') dt'$$

Since, the beam of electrons are irradiated during 5.3 sec, we evaluate $\lambda(\vec{r})$ which relates the initial distribution of order parameter $\eta(\vec{r}, t)$ for phase-field modeling (PF). $\lambda(\vec{r})$ is the normalized interpolation function of $E^d(\vec{r})$. When

$$\begin{cases} \lambda(\vec{r}) \leq 0.15 & \eta(\vec{r}, t = 5.3 \text{ sec}) = 0.45 \\ \lambda(\vec{r}) > 0.15 & \eta(\vec{r}, t = 5.3 \text{ sec}) = 0.90 \end{cases}$$

for realistic description of gelation process.

Subsequently, the results from the particle transport simulation, along with fixed experimental parameters such as radiation exposure time, battery weight, and absorbed dose, are processed to convert them into values suitable for multi-physics simulations. This data conversion ensures that the results are accurately representative of the actual experimental conditions and can be directly applied to subsequent simulations.

Phase-field modeling (PF) is performed to simulate the liquid-to-gel (gelation) phase transition with the energy deposited after electron irradiation at 5.3 sec as input, and the results ($\eta(\vec{r}, t)$) are coupled with thermal analysis (TA-2) of the electrolyte region concurrently. In the $t > 5.3$ s time interval, the multiphysics simulation between PF and TA-2 is performed using COMSOL software, and

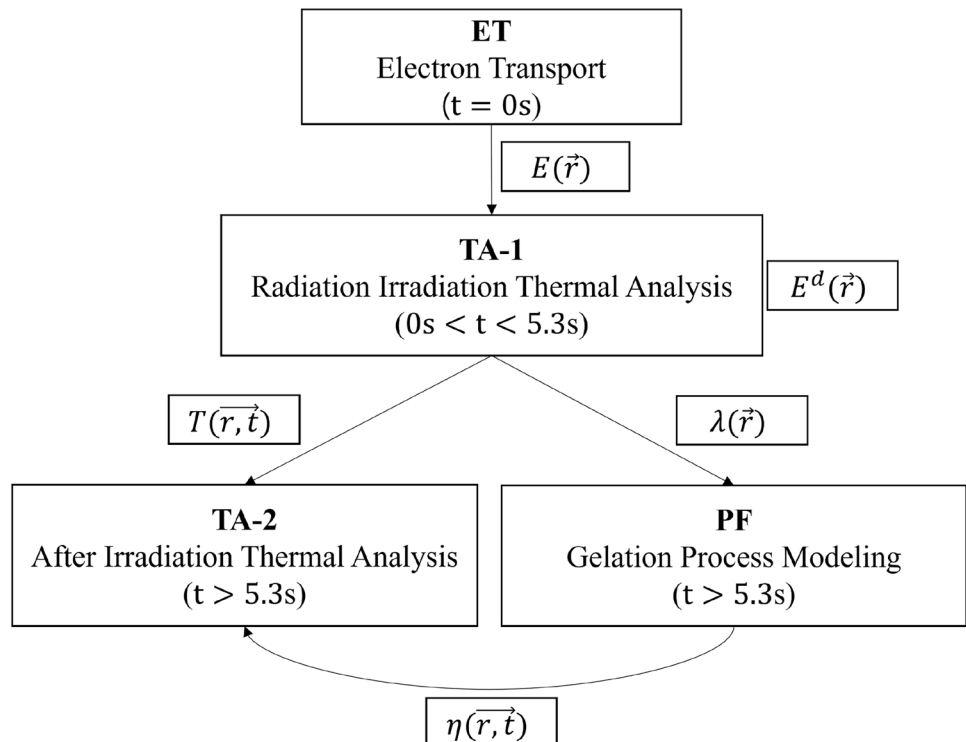
the location-dependent deposited energy information obtained from the radiation transport modeling performed at $0 \text{ s} < t < 5.3 \text{ s}$ is exported in the form of a csv (comma-separated values) file and used as initial data. Technically, we assume that the electron irradiation ends at $t = 0 \text{ s}$, and for $0 \text{ s} < t < 5.3 \text{ s}$, we only perform TA-1 modeling to release the deposited energy on a location-by-location basis to obtain a smoother temperature profile. The overall strategy of the multi-physics simulations of TA-1, PF, and TA-2 using COMSOL software based on the electron transport modeling is depicted in Fig. 3. When $t > 5.3 \text{ s}$, the simulation models the gelation process resulting from the interaction between the electron beam and the electrolyte. The evolution of thermal properties according to the degree of gelation is incorporated. Additionally, the heat generated during the chain growth polymerization process is also considered in the final thermal analysis.

Electron Beam Irradiation Simulation

Figure 4 shows an approximate depiction of the trajectory and shape of the electron beam irradiation simulated using Geant4, and it is a result obtained during the ET process in this study.

In the GEANT4-used radiation transport simulation (ET), a G4Box with a side length of 50 cm is used as the world volume. The material of the world is designed as air. The internal components of the LIB are constructed based on the dimensions listed in Table 1. The materials used in the

Fig. 3 Overview of simulations strategy



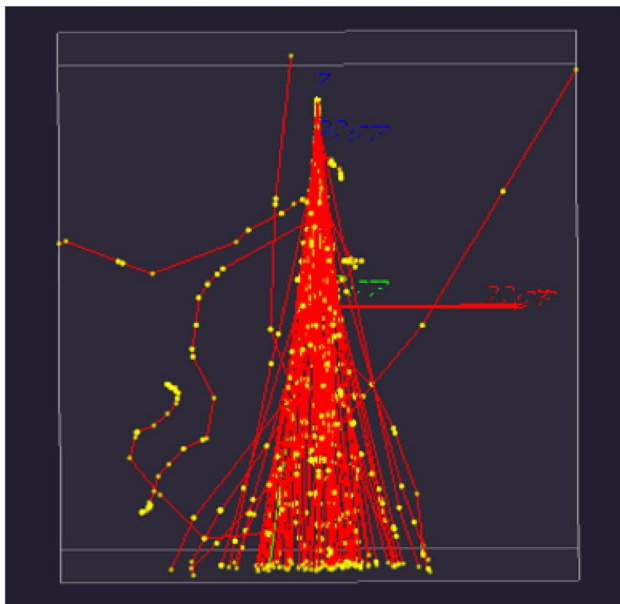
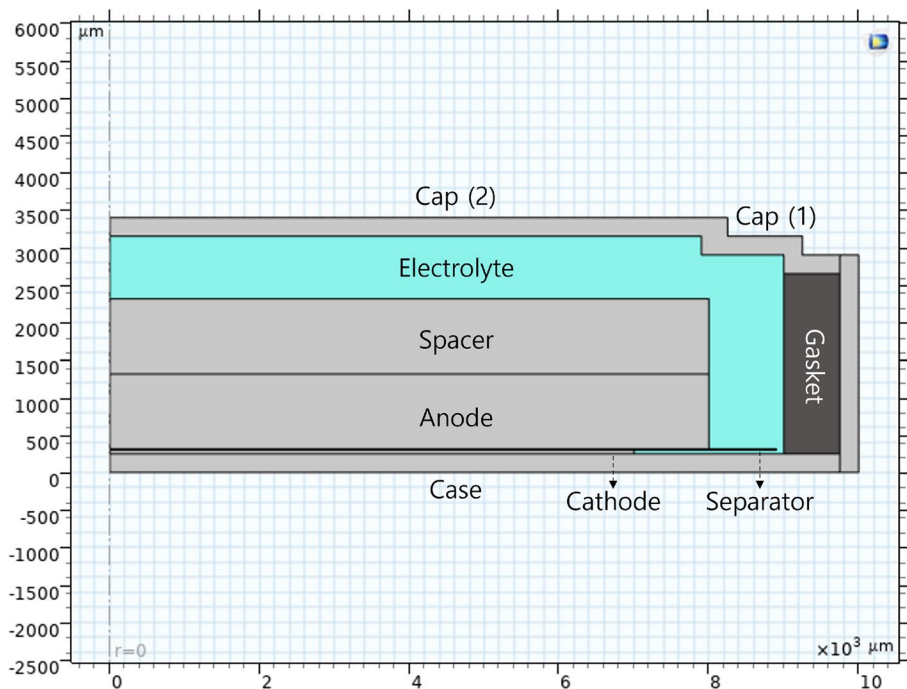


Fig. 4 Simulation of electron beam irradiation with 100 particles using GEANT4

electrolyte or electrodes are novel and have complex compositions, so custom definitions are created for all materials except Li, Poly(propylene), and air. While the LIB components are typically in contact and compressed during manufacturing, the simulation required adjustments to overlapping components such as the gasket and separator to avoid overlaps.

Fig. 5 Schematic geometry of the model. Constructing the 3D model by revolving the 2D model around the left gray dashed line

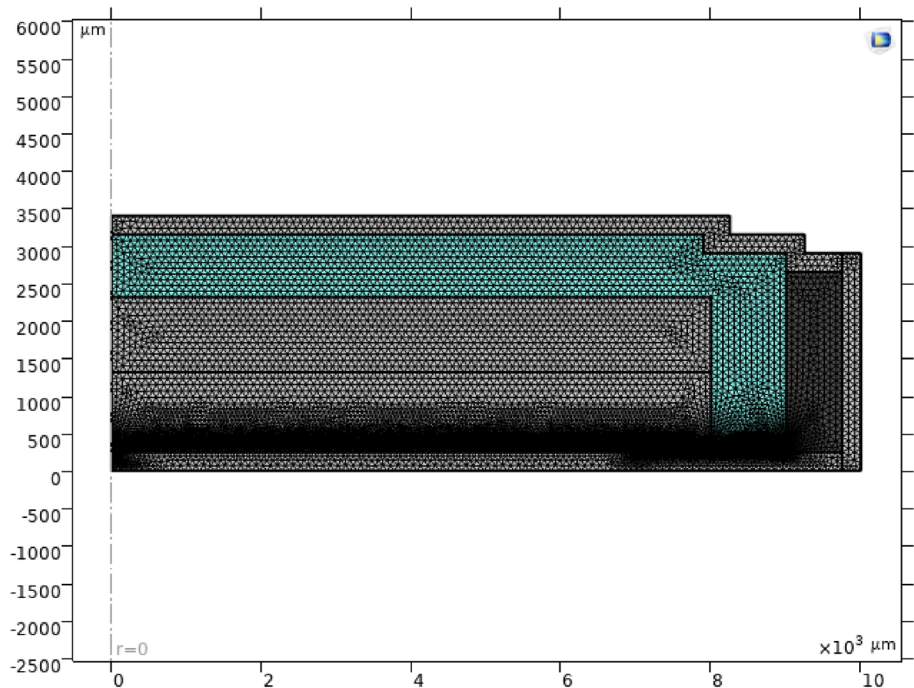


The radiation source is defined as an electron beam with an energy of 2.5 MeV, represented by the G4Electron class. The particle energy is set to 2.5 MeV, and the initial position is specified as G4ThreeVector(0, 0, 20 cm), ensuring that the source is located 35 cm above the lowest point in the z-axis at -15 cm. To ensure that the radiation is directed downward, rather than isotropically, the particle momentum direction is set to G4ThreeVector(0, 0, -1 cm).

GEANT4 allows the selection of an appropriate physics list based on the model to be analyzed. In this study, the QBBC physics list is used. QBBC is known for its excellent reproducibility in experiments involving particles with energies below 1 GeV colliding with thin targets, and includes standard electromagnetic(EM) processes. This makes it well suited to analyzing the interaction of 2.5 MeV electrons with the approximately 3 mm thick LIB components.

The simulation was conducted with enough particles to ensure reliable results. It was observed that the energy deposited per particle reached a saturation point with more than 10,000 particles. Therefore, for computational cost and to ensure the accuracy of the Monte Carlo method, 100,000 particles were generated. The entire simulation time was 71.82 s in real time. The electron transport simulation provided the deposited energy values due to interactions between the electron beam and the materials, along with their corresponding spatial coordinates.

Fig. 6 Mesh of geometry



Multi-physics Simulation

This section describes simulations TA-1, PF and TA-2. The model geometry is a 2D axis-symmetric geometry as shown in Fig. 5. The blue area is electrolyte which is completely filled in the LIB. The mesh of geometry is shown in Fig. 6 has the element size set to extremely fine.

Phase Field Modeling of the Gelation Process

To simulate the gelation process, we solve the Allen-Cahn equation [25], shown in Eq. 2. Since COMSOL software does not provide a dedicated module for this equation, we use the Coefficient PDE module. The Allen-Cahn equation is applied to the electrolyte domain to model the gelation process of LE. Order parameter, $\eta(\vec{r}, t)$ represents the degree of gelation. $\eta(\vec{r}, t) = 0$ means liquid electrolyte and $\eta(\vec{r}, t) = 1$ means the gel electrolyte and a value between 0 and 1 indicates the intermediate state between the liquid and gel electrolytes.

$$\frac{\partial \eta}{\partial t} = -M_\eta \left[\frac{\delta F}{\delta \eta} \right] \tag{2}$$

Here Eq. 2 is known as Allen-Cahn equation, a diffusion equation especially used for non-conserved order parameters. Equation 3 represents the total free energy of the domain Ω which adopts a simple double-well potential. M_η

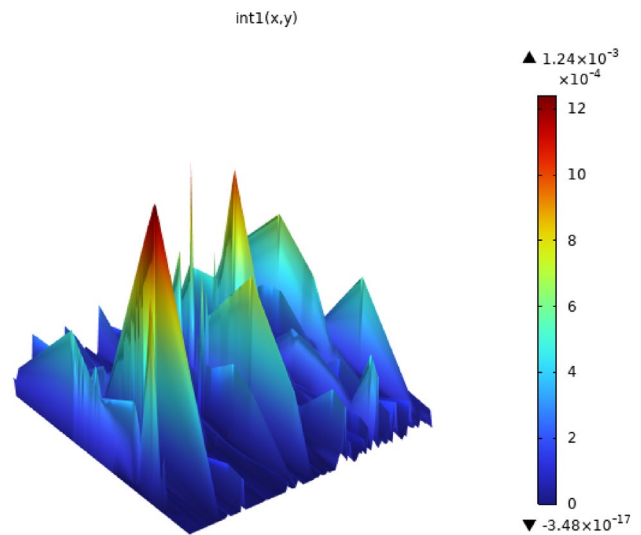


Fig. 7 Interpolation function of $E(\vec{r})$ csv file, where $E^d(\vec{r})$ indicates and the unit is J. Linear interpolation is applied within the range and no extrapolation is applied outside the range

relates to the interfacial mobility, $M_\eta = 1$ is used. ϵ , which governs the interfacial energy, is used in this study is 10^{-6} .

$$F = \int_{\Omega} \left[\frac{1}{2} \eta^2 (1 - \eta)^2 - \frac{\epsilon^2}{2} |\nabla \eta|^2 \right] d\Omega \tag{3}$$

As a boundary condition, we assume no reaction at the boundary, so we use a zero flux condition, as depicted in

Eq. 4. Figure 7 presents the results of deposited energy at various positions from the ET modeling, which were reprocessed into a CSV file format for use in COMSOL and plotted using the interpolation function in COMSOL.

$$-\mathbf{n} \cdot (-\nabla)\eta = 0 \quad (4)$$

Thermal Analysis

For the thermal analysis, the COMSOL internal Heat Transfer in the Solids and Fluid Module is used, which is chosen to analyze the temperature between the liquid electrolyte and the internal solid components. The following governing equations are used to solve for heat conduction inside the coin cell battery (Eqs. 5 and 6) and convection outside the battery (Eq. 7).

$$\rho(\eta)C_p(\eta)\frac{\partial T}{\partial t} + \rho(\eta)C_p(\eta)\mathbf{u} \cdot \nabla T + \nabla \cdot \mathbf{q} = Q_i \quad (i = 1, 2) \quad (5)$$

$$\mathbf{q} = -k(\eta)\nabla T \quad (6)$$

where

$$\begin{aligned} \rho(\eta) &= (1 - \eta)\rho_{liq} + \eta\rho_{gel} \\ C_p(\eta) &= (1 - \eta)C_{p,liq} + \eta C_{p,gel} \\ k(\eta) &= (1 - \eta)k_{liq} + \eta k_{gel} \end{aligned}$$

where properties of gel and liquid are listed in Table 2.

$$-\mathbf{n} \cdot \mathbf{q} = h(T_{ext} - T) \quad (7)$$

Where $h(\text{W}/\text{m}^2 \cdot \text{K})$ is the heat transfer coefficient, it is known to have a range of approximately 2.5 to 25 for air free convection [26]. For a conservative evaluation, we use the median value of $h = 10\text{W}/\text{m}^2 \cdot \text{K}$ in this study. T_{ext} (K) is external temperature which is initially set to 293.15K.

Q_1 for TA-1 simulation in right-hand side of Eq. 5 represents the total heat source which corresponds to the thermal analysis during the 5.3 s of electron beam irradiation, derived from the energy imparted by the electron beam as indicated in Eq. 8. The constant a in Eq. 8 is adjusted to match the absorbed dose of 10 kGy.

In TA-2 simulation, Q_2 shown in Eq. 9 is the total heat source that represents the heat generated during the chain growth polymerization in the gelation process of LE.

$$Q_1 = a \cdot \frac{E^d(\vec{r})}{t_{irr}} \quad (8)$$

$$Q_2 = \frac{1}{V} \left[\Delta H_{chain} \cdot \frac{\partial \eta}{\partial t} \right] \quad (9)$$

During the chain growth polymerization process, unsaturated monomers are added one by one to activated sites, leading to the growth of polymer chains. This process involves the conversion of the monomer's double bond (π -bond) into single bonds (σ -bonds) within the polymer, typically resulting in a decrease in enthalpy by approximately -8 to $-20 \text{ kcal}/\text{mol}$ [27, 28]. This transformation is generally known to be an exothermic reaction. In this study, since it is not feasible to directly measure the enthalpy of the chain polymerization process, we adopt a commonly accepted value of $-20 \text{ kcal}/\text{mol}$. For the thermal analysis, this value corresponds to $\Delta H_{chain} = 229.02 \text{ J}$.

Result

In this section, we present the results of the multiphysics analysis over time. Firstly, we will discuss the results of TA-1, followed by the results of PF and TA-2 for subsequent time periods.

Prior to discussing the results of the thermal analysis and phase field modeling of the gelation process, it is first necessary to define the maximum allowable temperature. The electrolyte material utilized in this study was 1 M LiTFSI in EC/EMC with ETPTA. Accordingly, an investigation was conducted to evaluate the highest temperature that each material is capable of withstanding. One advantage of LiTFSI is that it decomposes at temperatures above $300 \text{ }^\circ\text{C}$ [29]. The initial decomposition temperature of EC/EMC (1:1) was determined to be $205 \text{ }^\circ\text{C}$ [30], while the temperature at which the thermal stability of ETPTA crosslinked using UV was maintained approximately $350 \text{ }^\circ\text{C}$ [31]. Based on the aforementioned information, it was anticipated that the maximum allowable temperature would be approximately $200 \text{ }^\circ\text{C}$.

The temperature change in the LIB due to electron beam irradiation is illustrated in Fig. 8. Starting from an initial state of 293 K, the temperature gradually increases, reaching a maximum of 301 K at 5.3 s, the point when the irradiation ends. This indicates an approximate temperature rise of 8 K.

The initial conditions for the gelation simulation are set based on the $\lambda(\vec{r})$ in the electrolyte, resulting in varying $\eta(\vec{r}, t)$ values depending on the location. Consequently, the gelation process starts in the form depicted in Fig. 9(a). As time progress, the gelation spreads to surrounding areas, and by approximately 17.75 s, the entire region has transformed into a gel state shown in Fig. 9(d).

The thermal analysis results of TA-2 modeling, which follow the conclusion of the radiation exposure period, demonstrate the exothermic reactions that occur due to gelation and the alterations in material properties that are associated with the gelation process.

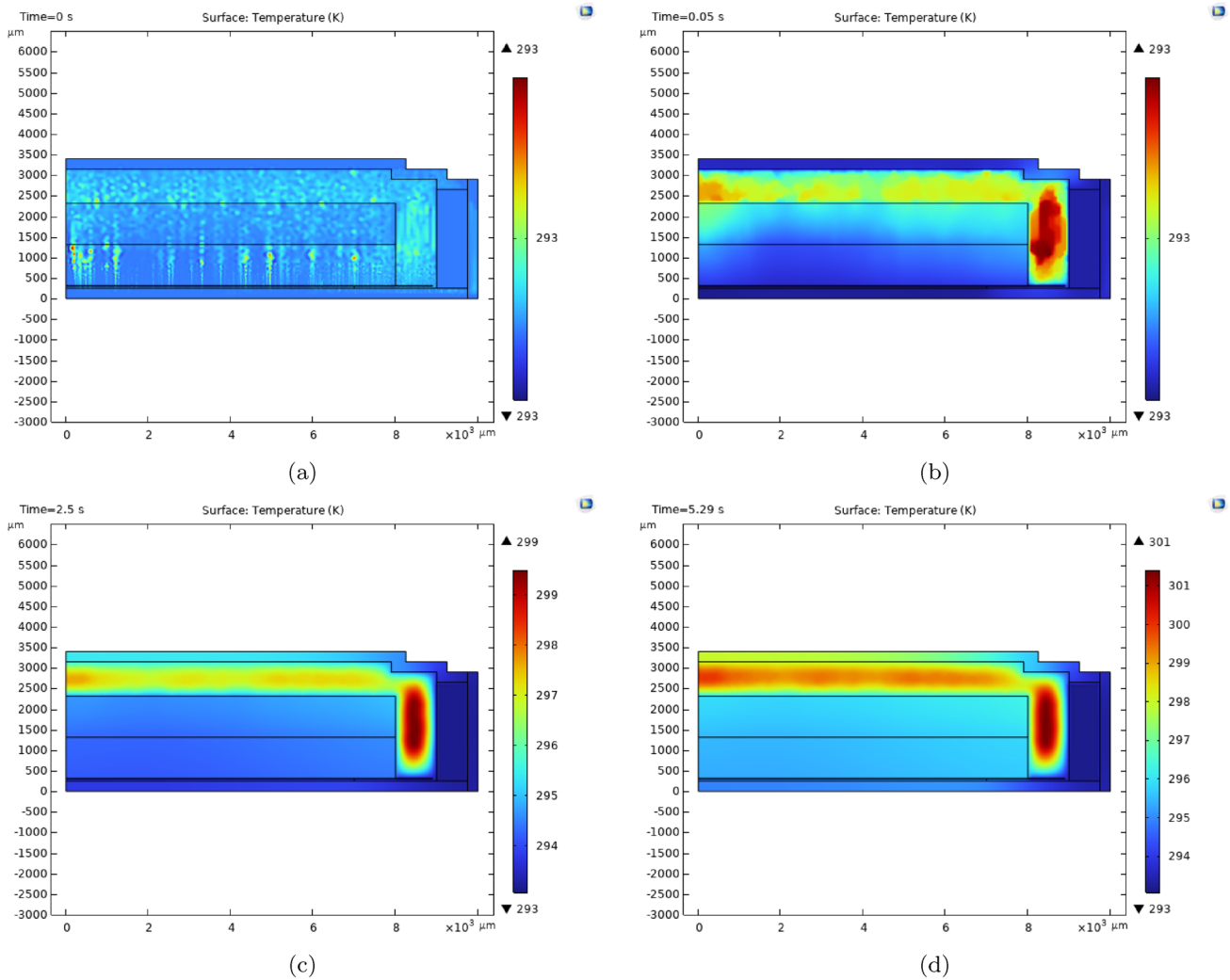


Fig. 8 Illustration of temperature distribution during radiation irradiation (TA-1). **a** $t = 0$ s, **b** $t = 0.05$ s, **c** $t = 2.5$ s, and **d** $t = 5.29$ s

The temperature rises from 301 to 319 K in 0.05 s shown in Fig. 10(a), beginning from the post-irradiation temperature. Subsequently, the temperature declines until approximately 1.8 s, after which continuous result in a further increase in temperature. The temperature reaches a maximum of approximately 349 K at 7.4 s after irradiation. Afterwards, the temperature declines gradually due to natural convection cooling, reaching approximately 298 K around 60 s.

The temperature graphs depicted in Fig. 11 have been calculated using the experimentally determined thermal properties (Table 2) of the electrolyte. Given that the outcomes of the TA may fluctuate in dependence upon the

value of the measured thermal property, a basic sensitivity analysis was conducted. A sensitivity analysis was conducted by varying the specific heat and thermal conductivity of the electrolyte by 10%, and the results are presented in Fig. 12. The results demonstrate that there were no considerable discrepancies in the recovery period. However, a 10% reduction in thermal properties resulted in a peak temperature increase of approximately 7 K (illustrated by the red solid line), while a 10% enhancement in thermal properties led to a decrease of approximately 4 K (illustrated by the red dashed line).

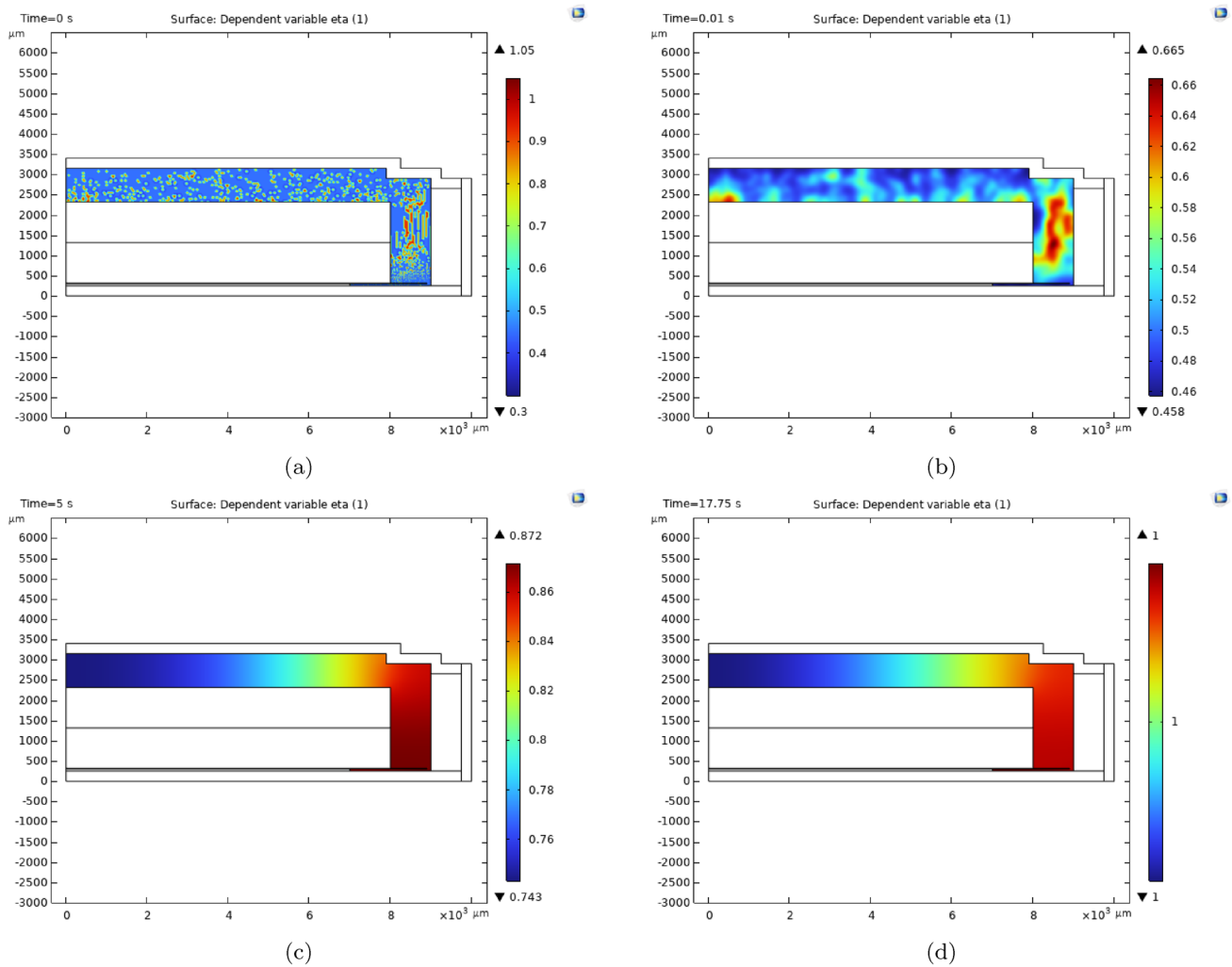


Fig. 9 Illustration of gelation progress over time (PF). **a** $t = 0$ s, **b** $t = 0.01$ s, **c** $t = 5$ s, and **d** $t = 17.75$ s

As commercial LIBs are becoming increasingly diverse in configuration and size, further analysis was performed. This additional analysis was carried out on a coin cell that is twice the size of the current simulation, with the system dimension, such as the radius of all components doubled and the absorbed dose of the battery increased

to 20kGy. The results of this supplementary analysis are shown in Fig. 13. When the size was doubled, the maximum temperature reached 377 K and the recovery time was approximately 100 s.

This outcome can be attributed to the fact that the system dimension has undergone a two-times expansion, accompanied by a significant rise in the probability of the reaction, as determined through radiation transport

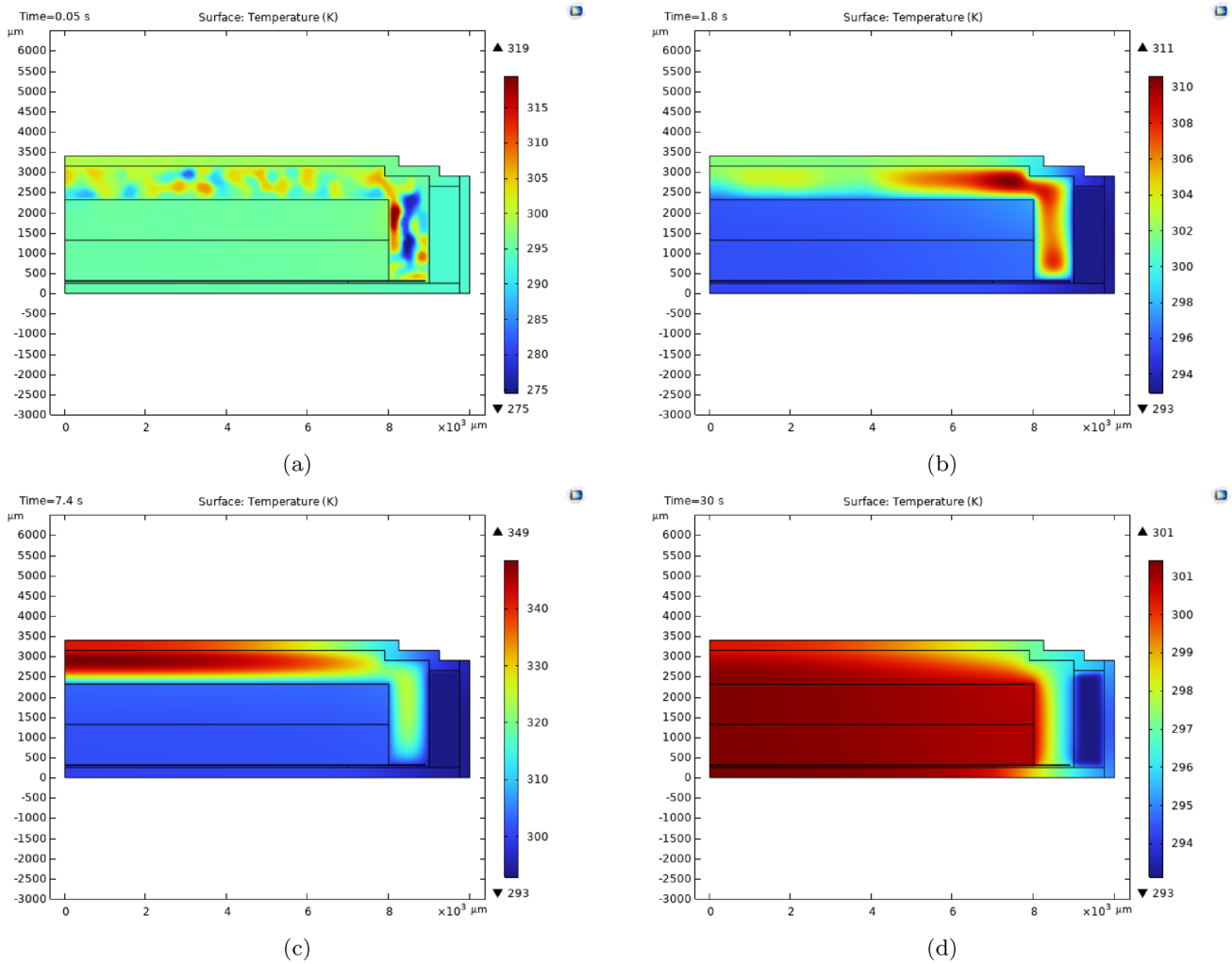


Fig. 10 Illustration of temperature change after radiation irradiation (TA-2). **a** $t = 0.05$ s, **b** $t = 1.8$ s, **c** $t = 7.4$ s, and **d** $t = 30$ s

modeling using GEANT4. Figure 14 illustrates the initial value of η , which is imported from the ET. A high initial η value may influence subsequent calculations of TAs and PF; therefore, it is important to ensure an accurate and representative η value at the outset. Furthermore, the complete gelation of the electrolyte took 10.75sec, a

shorter time than that observed for the reference simulation (17.75sec). Figure 14 is a comparison of the initial states of the gelation process between the reference size and the doubled size, based on data obtained through the ET process.

Fig. 11 Maximum temperature in LIB during the gelation process

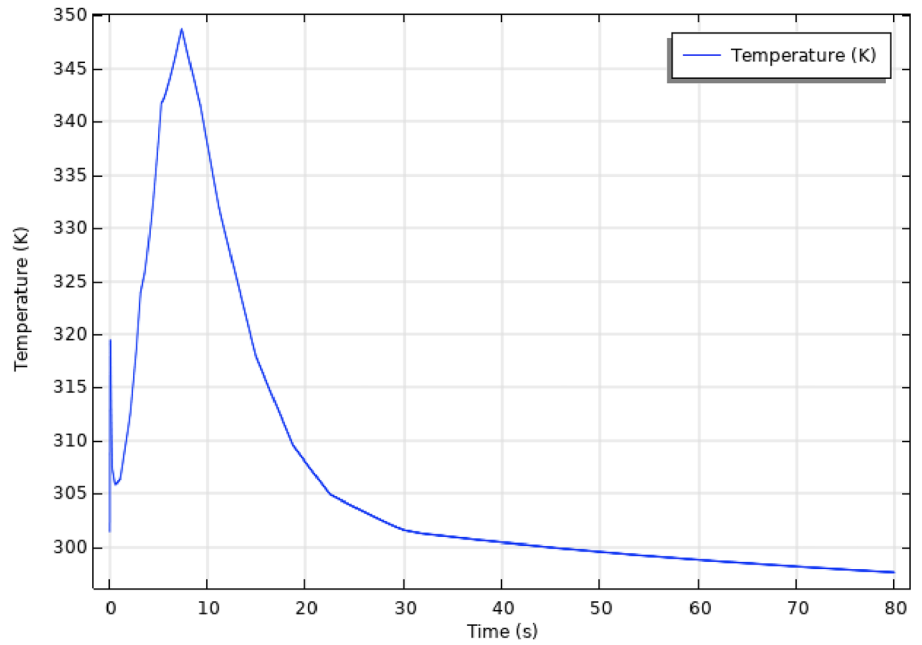


Fig. 12 Impact of electrolyte specific heat (C_p) and thermal conductivity(k) variations on maximum temperature during gelation process

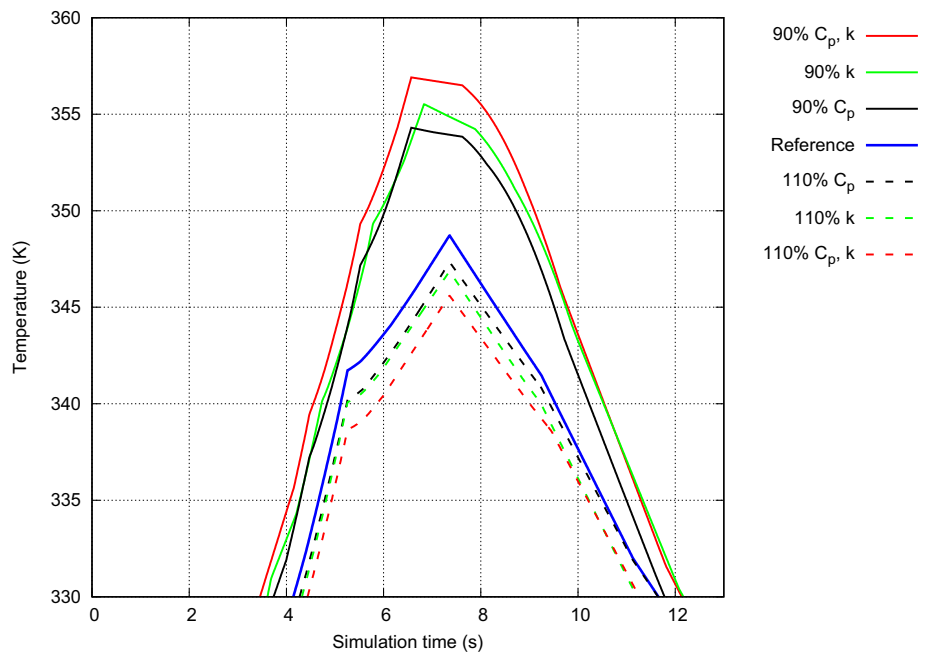


Fig. 13 Maximum temperature comparison of reference and doubled size LIB during the gelation process

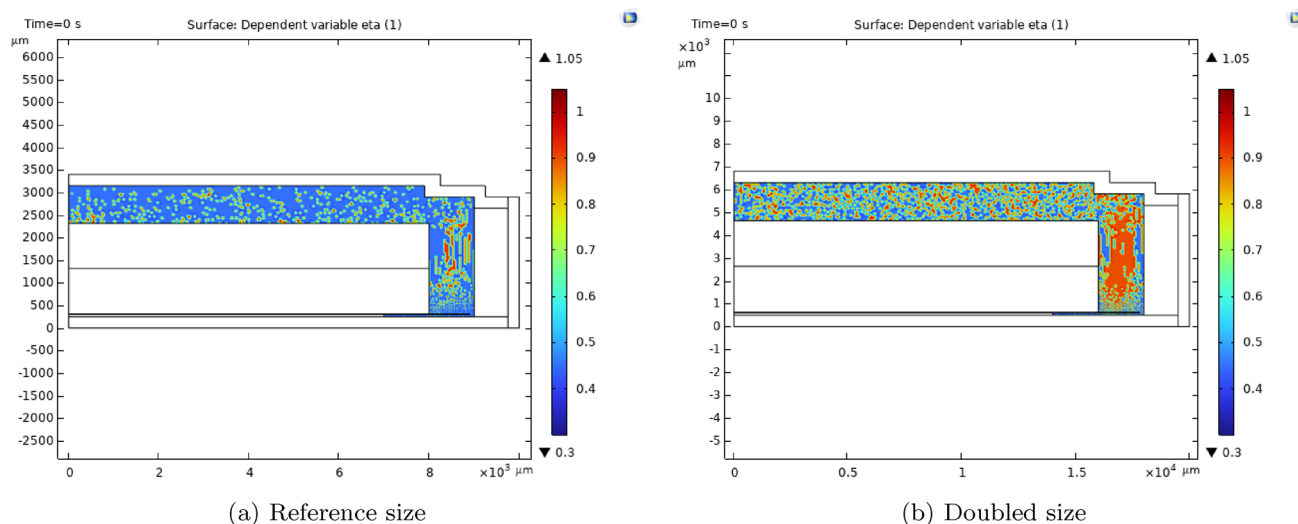
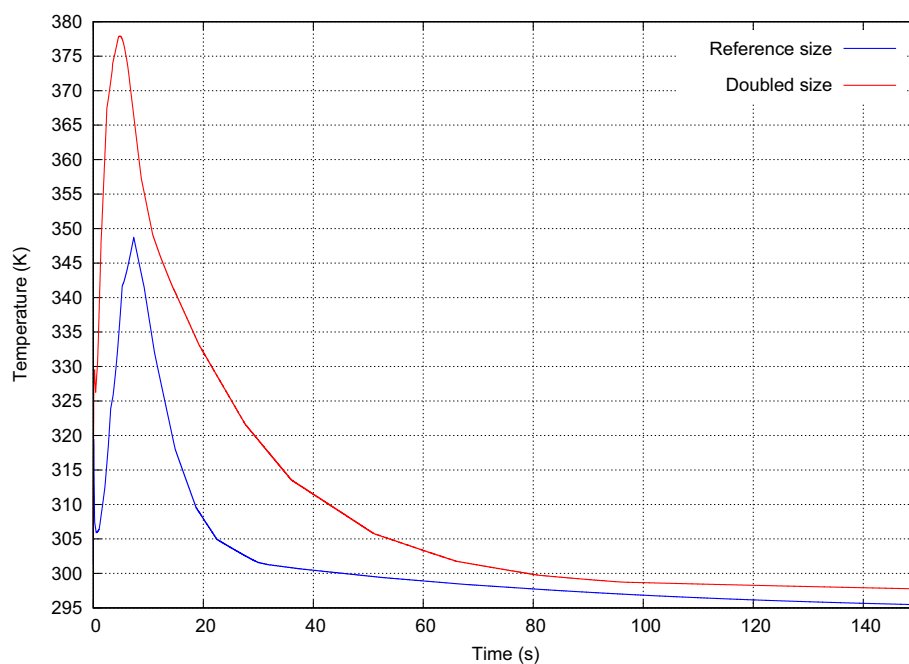


Fig. 14 Comparison of $\eta(\vec{r})$ initial state between reference and doubled size

Conclusions

A multiphysics simulation was performed to simulate the gelation process by electron irradiation coupled with electron transport modeling and thermal analysis of the gelation process of the polymer electrolyte of the lithium-ion battery. Through the simulation, it was confirmed that phenomena at different scales of time and space can be coupled and interpreted, and the behavior of the polymer electrolyte in the coin cell, which cannot be seen inside, can

be reasonably predicted. When irradiated with a 10 kGy electron beam for 5.3 sec at temperature of 293 K, the peak temperature was 349 K, and the temperature returned to room temperature (298 K) after about 60 s. The proposed multiphysics simulation strategy in this study can be extended to GPEs with different thermal properties and lithium ion batteries of different form factors.

Acknowledgements This work was supported by the National Research Foundation of Korea (NRF) Grant funded by the Korean Government (MSIT) RS-2022-00154546. This work was also supported by Korea Institute of Energy Technology Evaluation and Planning (KETEP)

grant funded by the Korea government (MOTIE) (RS-2024-00349003, Support for on-site practical training linked to public enterprises).

Data availability The processed data required to reproduce these findings would be available upon the request.

References

- M. Sanders, Lithium-ion battery raw material supply and demand 2016–2025. In *Document presentado en the “Advanced Automotive Battery Conference”, San Francisco*, (2017)
- K. Amine, R. Kanno, Y. Tzeng, Rechargeable lithium batteries and beyond: Progress, challenges, and future directions. *MRS Bull.* **39**(5), 395–401 (2014)
- Q. Wang, P. Ping, X. Zhao, G. Chu, J. Sun, C. Chen, Thermal runaway caused fire and explosion of lithium ion battery. *J. Power Sources* **208**, 210–224 (2012)
- V. Aravindan, J. Gnanaraj, S. Madhavi, H.-K. Liu, Lithium-ion conducting electrolyte salts for lithium batteries. *Chem-A Eur J* **17**(51), 14326–14346 (2011)
- Qingsong Wang, Lihua Jiang, Yu. Yan, Jinhua Sun, Progress of enhancing the safety of lithium ion battery from the electrolyte aspect. *Nano Energy* **55**, 93–114 (2019)
- J.-M. Tarascon, M. Issues and challenges facing rechargeable lithium batteries. *Nature* **414**(6861), 359–367 (2001)
- N. Rane, S. Choudhary, J. Rane, Enhancing lithium-ion battery performance with emerging electrolyte materials for sustainable energy storage solutions: a comprehensive review and prospects. *Available at SSRN 4643648*, (2023)
- N. Badi, A.M. Theodore, S.A. Alghamdi, H.A. Al-Aoh, A. Lakhout, P.K. Singh, M.N. Norrahim, G. Nath, The impact of polymer electrolyte properties on lithium-ion batteries. *Polymers* **14**(15), 3101 (2022)
- A. Manuel Stephan, Review on gel polymer electrolytes for lithium batteries. *Eur. Polym. J.* **42**(1), 21–42 (2006)
- J. Ma, Z. Wang, W. Jinghua, G. Zhi, X. Xin, X. Yao, In situ solidified gel polymer electrolytes for stable solid-state lithium batteries at high temperatures. *Batteries* **9**(1), 28 (2022)
- A.M. Christie, S.J. Lilley, E. Staunton, Y.G. Andreev, P.G. Bruce, Increasing the conductivity of crystalline polymer electrolytes. *Nature* **433**(7021), 50–53 (2005)
- S.D. Tillmann, P. Isken, A. Lex-Balducci, Gel polymer electrolyte for lithium-ion batteries comprising cyclic carbonate moieties. *J. Power Sources* **271**, 239–244 (2014)
- S. Jankowsky, Martin M. Hiller, O. Fromm, M. Winter, H.-D. Wiemhöfer, Enhanced lithium-ion transport in polyphosphazene based gel polymer electrolytes. *Electrochim. Acta* **155**, 364–371 (2015)
- D. Zhou, Y.B. He, Q. Cai, X. Qin, B. Li, H. Du, Q.H. Yang, F. Kang, Investigation of cyano resin-based gel polymer electrolyte: in situ gelation mechanism and electrode-electrolyte interfacial fabrication in lithium-ion battery. *J. Mater. Chem. A* **2**(47), 20059–20066 (2014)
- Shih-Hong. Wang, Ping-Lin. Kuo, Chien-Te. Hsieh, Hsiehsheng Teng, Design of poly (acrylonitrile)-based gel electrolytes for high-performance lithium ion batteries. *ACS Appl. Mater. Interfaces.* **6**(21), 19360–19370 (2014)
- V. Vijayakumar, B. Anothumakkool, S. Kurungot, M. Winter, J.R. Nair, In situ polymerization process: an essential design tool for lithium polymer batteries. *Energy Environ. Sci.* **14**(5), 2708–2788 (2021)
- Seokyoung Park, Joon-Yong. Sohn, In-Tae. Hwang, Junhwa Shin, Jin-Mun. Yun, KwangSup Eom, Kwanwoo Shin, Young-Moo. Lee, Chan-Hee. Jung, In-situ preparation of gel polymer electrolytes in a fully-assembled lithium ion battery through deeply-penetrating high-energy electron beam irradiation. *Chem. Eng. J.* **452**, 139339 (2023)
- J.P. Collier, B.H. Currier, F.E. Kennedy, J.H. Currier, G.S. Timmins, S.K. Jackson, R.L. Brewer, Comparison of cross-linked polyethylene materials for orthopaedic applications. *Clin. Orthop. Relat. Res.* **414**, 289–304 (2003)
- M. Ueno, N. Imanishi, K. Hanai, T. Kobayashi, A. Hirano, O. Yamamoto, Y. Takeda, Electrochemical properties of cross-linked polymer electrolyte by electron beam irradiation and application to lithium ion batteries. *J. Power Sources* **196**(10), 4756–4761 (2011)
- L. Spitthoff, P.R. Shearing, O.S. Burheim, Temperature, ageing and thermal management of lithium-ion batteries. *Energies* **14**(5), 1248 (2021)
- T.M. Bandhauer, S. Garimella, T.F. Fuller, A critical review of thermal issues in lithium-ion batteries. *J. Electrochem. Soc.* **158**(3), 1 (2011)
- Shuai Ma, Modi Jiang, Peng Tao, Chengyi Song, Wu. Jianbo, Jun Wang, Tao Deng, Wen Shang, Temperature effect and thermal impact in lithium-ion batteries: A review. *Progress Nat. Sci.: Mater. Int.* **28**(6), 653–666 (2018)
- S. Agostinelli, J. Allison, K.A. Amako, J. Apostolakis, H. Araujo, P. Arce, M. Asai, D. Axen, S. Banerjee, G.J. Barrand, F. Behner, G.J.N.I. Barrand et al., Geant4-a simulation toolkit. *Nuclear Instrum. Methods Phys. Res. Sect. A: Accel. Spectrom. Detect. Assoc. Equip.* **506**(3), 250–303 (2003)
- Long-Qing. Chen, Phase-field models for microstructure evolution. *Annu. Rev. Mater. Res.* **32**(1), 113–140 (2002)
- S.M. Allen, J.W. Cahn, A microscopic theory for antiphase boundary motion and its application to antiphase domain coarsening. *Acta Metall.* **27**(6), 1085–1095 (1979)
- John Malmqvist, Edward, F. Crawley, *Exploring Engineering: An Introduction to Engineering and Design*. Elsevier, (2013)
- C Schaller, *Polymer Chemistry*, chapter 3. Kinetics and Thermodynamics of Polymerization. Chemistry LibreTexts, Accessed: 2023-06-08 (2023)
- Sergey Vyazovkin, Dimitris Achilias, Xavier Fernandez-Francos, Andrey Galukhin, Nicolas Sbirrazzuoli, Ictac kinetics committee recommendations for analysis of thermal polymerization kinetics. *Thermochim. Acta* **714**, 179243 (2022)
- Lu. Zhenrong, Li. Yang, Yaju Guo, Thermal behavior and decomposition kinetics of six electrolyte salts by thermal analysis. *J. Power Sources* **156**(2), 555–559 (2006)
- Emc electrolyte for lithium ion batteries, Gerardine G Botte, Ralph E White, and Zhengming Zhang. Thermal stability of lipf6-ec. *J. Power Sources* **97**, 570–575 (2001)
- Ruiping Liu, Wu. Zirui, Peng He, Haoyu Fan, Zeya Huang, Lei Zhang, Xinshuang Chang, Hang Liu, Chang-an Wang, Yutao Li, A self-standing, uv-cured semi-interpenetrating polymer network reinforced composite gel electrolytes for dendrite-suppressing lithium ion batteries. *J. Materiomics* **5**(2), 185–194 (2019)

Publisher's Note Springer Nature remains neutral with regard to jurisdictional claims in published maps and institutional affiliations.

Springer Nature or its licensor (e.g. a society or other partner) holds exclusive rights to this article under a publishing agreement with the author(s) or other rightsholder(s); author self-archiving of the accepted manuscript version of this article is solely governed by the terms of such publishing agreement and applicable law.